Physics of Fluids

An analytic probability density function for partially premixed flames with detailed chemistry

Cite as: Phys. Fluids **33**, 035117 (2021); https://doi.org/10.1063/5.0038888
Submitted: 30 November 2020 • Accepted: 15 January 2021 • Published Online: 05 March 2021

M. Pfitzner and P. Breda

Physics of Fluids ARTICLE scitation.org/journal/phf

An analytic probability density function for partially premixed flames with detailed chemistry

Cite as: Phys. Fluids **33**, 035117 (2021); doi: 10.1063/5.0038888
Submitted: 30 November 2020 · Accepted: 15 January 2021 ·
Published Online: 5 March 2021

M. Pfitzner[a] and P. Breda

AFFILIATIONS

Thermodynamics Institute LRT-10, Bundeswehr University Munich, Werner-Heisenberg-Weg 39, 85579 Neubiberg, Germany

Note: This paper is part of the Special Topic, In Memory of Edward E. (Ted) O'Brien.
[a]**Author to whom correspondence should be addressed:** michael.pfitzner@unibw.de

ABSTRACT

Laminar premixed flame profiles of methane/air free flames and strained flames at different fuel/air ratios and strain rates are analyzed using detailed chemistry with Lewis numbers equal to one. It is shown that the detailed chemistry flame profiles of progress variables $CO_2 + CO$ and $H_2O + H_2$ in canonically stretched coordinates can be fitted accurately by a slight generalization of recently proposed analytical presumed flame profiles over a wide range of fuel/air ratios through adaptation of a single model parameter. Strained flame profiles can be reproduced using an additional linear coordinate transformation, emulating the compression of the preheat zone by strain as predicted by premixed flame theory. The model parameter can alternatively be determined using only the laminar flame speeds and the fully burnt temperatures from the laminar flame calculations. The stretch factor of the coordinate transformation is proportional to cp/lambda, which drops by a factor up to 4 across the laminar flame. It is shown how the non-constant cp/lambda modifies the laminar flame probability density function (pdf) and a polynomial fit to cp/lambda as a function of the progress variable allows analytical results for the laminar flame pdf and the mean value of the progress variable and of the reaction source term. An analytic pdf for partially premixed flames is proposed based on Bayes's theorem as a combination of a beta pdf for the mixture fraction and the laminar flame pdf's evaluated at the respective fuel/air ratio.

I. INTRODUCTION

In many technical burners featuring the propagation of thin flame fronts, the mixture fraction field is not completely homogeneous. Then, flame fronts propagate through regions of varying fuel/air ratios, but the thermal flame thickness is usually much smaller than the inverse gradient of the mixture fraction. The reason is that small scale fluctuations of passive scalars such as mixture fraction die out very quickly due to diffusion, while the gradient of the progress variable within a propagating flame front is maintained by the interaction of diffusion and chemical reaction.

In computational fluid dynamics (CFD) simulations of such flames using Reynolds-averaged Navier–Stokes (RANS) simulations or Large Eddy Simulations (LESs), the size of computational cells is usually too big to fully resolve the laminar flame structure embedded in the turbulent flow field. The ratio of flame thickness to cell size decreases further at elevated pressures due to the drop of diffusivity and heat conductivity. Thus, subgrid combustion models are required for RANS simulations and LESs of most technical burners.

The propagating flame fronts are folded and stretched by the turbulent flow field. Experimental observations[1] and Direct Numerical Simulation (DNS) results[2] indicate that particularly at lower levels of turbulence intensity u'/s_L, the subgrid fuel consumption rate is increased proportionally to the amount of wrinkling of the reaction layer. Additional effects such as flame stretch, flame curvature, and thickening of the reaction layer through small scale turbulent eddies modify this proportionality only moderately. Even at quite large Karlovitz numbers, the inner structure of the reaction layer of hydrocarbon–air flames appears to remain largely intact.[3]

In many turbulent combustion models for premixed flames, a single normalized reaction progress variable c is invoked, which is zero (one) in the fully unburnt (burnt) regions. c might be defined from the normalized temperature rise or by some combination of educt or product species. The local chemical state is well characterized by such a single progress variable as long as the inner flame structure is not strongly modified by turbulent mixing.

Premixed laminar flame profiles can be tabulated either as freely propagating flames or in a counterflow setting, where strained flames can be investigated. Once a monotonously rising progress variable is chosen, all other quantities can be calculated from such tables. (Quasi-)DNS calculations have been performed, where detailed chemistry was replaced by such flame generated manifold (FGM) tables of freely propagating premixed flames[4] while all turbulent eddies and the folding of the flame front were fully resolved.

Many turbulent premixed flame combustion subgrid models for LESs and RANS simulations have been developed in the past. The artificially thickened flame (ATF) model[5] makes the flame front resolvable on LES grids by increasing the diffusion coefficient and the heat conductivity while reducing the reaction term such that the local laminar flame propagation speed remains unchanged. The effect of non-resolved subgrid flame wrinkling is taken into account by an empirical efficiency function.

Some models assume the existence of an infinitely thin flame front propagating at a turbulent flame speed s_T, which is provided through a separate model. Examples are the G equation level-set approach[6] and subgrid flame surface density (FSD) models. In the latter, the sum of the molecular diffusion term and chemical reaction source term of the c transport equation is replaced by $\rho_u \langle s_c \rangle \Sigma_f$ with flame surface density Σ_f and a surface averaged flame speed $\langle s_c \rangle$. Σ_f is either determined by a transport equation[7] or approximated as $\Sigma_f = \Xi |\overline{\nabla c}|$, evoking algebraic models for the wrinkling factor Ξ[8] and often replacing $|\overline{\nabla c}|$ by $|\nabla \tilde{c}|$. Models of this type change the mathematical character of the progress variable transport equation, preventing recovery of the laminar flame front structure in the DNS limit.

In the framework of LES, the filtered laminar flame model pretabulates the chemical source term,[9] which is filtered from a flat laminar flame on a one-dimensional (1D) grid. The filter size for the tabulation is chosen either equal to the LES grid size Δ or even larger than Δ to avoid numerical oscillations. In the latter case, the chemical source term is smeared out over a larger number of cells in physical space. Incorporation of effects of subgrid flame folding, flame stretch, and flame thickening requires empirical modifications. Attempts to derive more accurate expressions for $\overline{\omega(c)}$ for an underresolved flat flame in LES cells by 1D approximate deconvolution have been reported in Ref. 10. The latter method is not easily generalizable to more than one spatial dimension and appears to require quite fine LES resolution.

In contrast to models developed specifically for premixed flames, pdf methods are formally applicable to all combustion regimes and to an arbitrary number of spatial dimensions. The structure of the subgrid flame front is reflected in the shape of the pdf, and this has not always been appreciated enough in the past. While pdf methods have been very successful in the modeling of non-premixed flames, the straightforward application of those methods to estimate the filtered source term in the c transport equation of premixed flames can yield inaccurate results.

The beta pdf is a good model pdf for pure diffusion processes, and it represents the standard subgrid pdf for mixture fraction in non-premixed flames. As a progress variable pdf in premixed flames, it has been shown to overestimate the mean reaction term for large c variance near the thin flame limit.[11] DNS analyses[12] showed good agreement between the DNS source term filtered to a LES grid and the beta pdf value (with mean and variance of the beta pdf evaluated from the DNS) only for small ratios of $\Delta_{LES}/\Delta_{DNS} < 5$, i.e., $\Delta_{LES} < \delta_{th}$, where δ_{th} is the thermal flame thickness.

Presumed premixed flame pdfs derived from filtering numerically generated 1D laminar flame profiles have been proposed in Refs. 11, 13, and 14. These authors invoked empirical cutoffs near $c = 0, 1$ to avoid numerical divergence of their integrals when calculating the normalization condition of the pdf and mean and variance of the progress variable. Domingo *et al.*[13] reported that such laminar flame pdf's with *ad hoc* choice of the integration limits c^-, c^+ delivered negative weights of the delta functions for small values of c variance. The authors used a beta pdf in those cases. Salehi *et al.*[14,15] presented a modified laminar flame pdf allowing its application to the whole range of c variances. The application of the (stochastic) linear eddy model to numerically derived 1D laminar flames[16] and evaluation of DNS data[17] showed pdf's with smeared-out cutoffs in the regions toward $c = 0, 1$. Postprocessing of experimental data of highly turbulent premixed flames[18] showed that the inner structure of the reaction zone and the profile of progress variable are little affected even at the very high turbulence levels investigated.

Subgrid progress variable pdf's were evaluated from DNS data by Moureau *et al.*[19] and Lapointe and Blanquart.[20] To gain a good agreement of the level of the DNS pdf's with 1D laminar flame pdf's, the latter were filtered using an effective filter width $\Delta' < \Delta$, which was calculated from the condition that the mean and variance evaluated with the 1D pdf agreed with those evaluated from the filtered DNS. Mean species concentrations were evaluated from DNS data by Lipatnikov *et al.*,[21–23] showing that beta pdf's and a flamelet pdf could generate good agreement with filtered DNS data for mean values of most species. The pdf scaled with an empirical factor[22] also agreed well with that evaluated from the DNS in a range of progress variables (PVs) centered around its mean value.

Analytical laminar flame shapes and pdf's can be evaluated when using appropriate surrogate reaction source terms instead of the complex Arrhenius one. A simple linear source term[24] was proposed in the 1990s; recently, a more accurate approximation to the Arrhenius single-step chemistry source term was introduced[25] and later improved.[26] All of these surrogate source terms generate analytical invertible flame profiles and laminar flame pdf's.

A simple two-dimensional sinusoidal flame folding model[25] revealed that flame wrinkling increases the level of the pdf in the reactive region while it is smeared out near the cutoffs near $c = 0, 1$. The increased level of the pdf in the reactive c region could be emulated through a laminar flame pdf evaluated with a reduced filter size $\Delta' = \Delta/\Xi$, where Ξ is the geometrical wrinkling factor of the folded reaction layer. This shows that the use of a (smaller) effective filter width in the work of Moureau and Lapointe/Blanquart effectively mimics the effect of subgrid flame wrinkling.

Similar pdf's were obtained[26] filtering RANS-like volumes using DNS data of premixed flames with one-step chemistry. The empirical factor multiplying the 1D pdf could be well reproduced by the procedure proposed by Moureau.[19] The filtered chemical reaction source term evaluated from one-step chemistry DNS[27] agreed well with the filtered source term calculated from the model analytic pdf scaled by a wrinkling factor, which is estimated using the isosurface area of the most reactive progress variable within the filter volume.

The goal of the present paper is to show that using an appropriately (canonically) stretched coordinate, premixed laminar methane–air flame profiles generated with detailed chemistry can be

represented very accurately through analytically defined, invertible flame profiles over a large range of fuel/air ratios and strain rates, providing analytical expressions for mean values of the progress variable, reaction source term, and laminar flame pdf.

This paper is structured as follows: First, we present the progress variable transport equation and recall some ingredients of single-step Arrhenius chemistry and the canonical transformation of the spatial coordinate. After introduction of the analytical presumed flame profile and pdf, we describe the calculation of the premixed laminar flame profiles using detailed chemistry. We discuss the process of fitting the model parameter to the flame profile and laminar flame speed and derive correlations for use in actual simulations. We then propose a 2D analytical presumed pdf $p(Z, c)$ for partially premixed flames based on Bayes's theorem and give some conclusions.

II. TRANSPORT EQUATION OF PROGRESS VARIABLE

In flames where thin premixed flame fronts are propagating through a (potentially inhomogeneous) mixture, it is common to use a single reaction progress variable, which is often chosen as $c = (T - T_u)/(T_b - T_u)$ in the homogeneous mixtures at constant pressure. T_u, T_b are the unburnt and fully burnt temperatures, respectively. Alternatively, a suitable combination of concentrations of chemical species can be chosen, which may be more suitable in the inhomogeneous case due to the dependence of T_b on the fuel/air ratio. The one-dimensional c transport equation is given by[7]

$$\rho\frac{\partial c}{\partial t}+\rho u\frac{\partial c}{\partial x}=\frac{\partial}{\partial x}\left(\frac{\lambda}{c_p}\frac{\partial c}{\partial x}\right)-\frac{\dot{\omega}_F}{Y_F}, \tag{1}$$

where ρ, u, c are the density, velocity, and progress variable and λ, c_p are the heat conductivity and specific heat at constant pressure. For Arrhenius chemistry and Lewis number $Le = 1$, the chemical source term can be written as[7]

$$\frac{\dot{\omega}_F}{Y_F}=B_1T^{\beta_1}e^{-\frac{\beta}{2}}\rho(1-c)\exp\left(-\frac{\beta(1-c)}{1-\alpha(1-c)}\right), \tag{2}$$

where $\alpha=\frac{T_b-T_u}{T_b}$ represents the normalized temperature rise and $\beta = \alpha T_a/T_b$ is a measure of the activation temperature T_a. The temperature exponent β_1 in Eq. (2) is usually taken as $\beta_1 = 0$ or $\beta_1 = 1$. For steady-state conditions, the continuity equation requires $\rho u = \rho_u s_L$, and we have $\rho \sim 1/T \sim 1/(1 - \alpha(1 - c))$ for constant pressure combustion.

For a stationary flame, Eq. (1) yields

$$\rho_u s_L\frac{\partial c}{\partial x}-\frac{\partial}{\partial x}\left(\frac{\lambda}{c_p}\frac{\partial c}{\partial x}\right)=\omega_x(c), \tag{3}$$

with $\omega_x(c)=-\frac{\dot{\omega}_F}{Y_F}$ and taking into account the continuity equation $\rho u = \rho_u s_L$. Rescaling the x coordinate according to $d\xi = \rho_u s_L c_p/\lambda dx$ as

$$\xi(x)-\xi_0=\rho_u s_L\int_{x_0}^{x}\frac{c_p(x')}{\lambda(x')}dx' \tag{4}$$

transforms Eq. (1) into canonical form,

$$\frac{\partial c}{\partial \xi}-\frac{\partial^2 c}{\partial \xi^2}=\omega(c), \tag{5}$$

with

$$\begin{aligned}\omega(c)&=\Lambda(1-\alpha(1-c))^{\beta_1-1}(1-c)\exp\left(-\frac{\beta(1-c)}{1-\alpha(1-c)}\right)\\&=\left(\frac{\lambda}{c_p}\right)\frac{\omega_x(c)}{(\rho_u s_L)^2}.\end{aligned} \tag{6}$$

The prefactor Λ in Eq. (6) represents the eigenvalue of the transport equation, which guarantees that the boundary conditions $c = 0$ for $\xi \to -\infty$ and $c = 1$ for $\xi \to +\infty$ are fulfilled.

If the progress variable is not normalized, i.e., $c = C$ for $\xi \to +\infty$ with $C \neq 1$, the source term is just multiplied by C, which represents the maximum of the progress variable in the fully burnt state. Note that c_p/λ is not constant in Eq. (4) for flame profiles calculated with detailed chemistry and realistic transport properties, leading to a nonlinear stretch transformation.

III. LAMINAR FLAME pdf's

A probability density function $p(c)$ allows for the evaluation of cell averages of arbitrary quantities $z(c)$ through $\overline{z(c)} = \int z(c)p(c)dc$. In classical Bray–Moss–Libby (BML) theory, the pdf is assumed to take the form

$$p_{BML}(c)=A\delta(c)+B\delta(1-c)+\gamma(c), \tag{7}$$

with $\gamma(c) \ll 1$. For $\gamma(c) \to 0$, one obtains $A \sim (1 - \bar{c})$ and $B \sim \bar{c}$. Since the chemical source term $\omega(c)$ vanishes at $c = 0, 1$, its mean cannot be evaluated from $p_{BML}(c)$ with $\gamma(c)$ set to zero. For a given $c(\xi)$ profile, the 1D laminar flame pdf $p(c)$ is given by[11,19,25]

$$p(c)=\frac{1}{N}\frac{1}{dc/d\xi}H(c-c^-)H(c^+-c), \tag{8}$$

where $H(x)$ is the Heaviside function and $c^- = c(\xi^-)$, $c^+ = c(\xi^+)$, with ξ^-, ξ^+ denoting the left and right boundaries of the filter interval. The denominator N guarantees the correct normalization of $p(c)$,

$$\int_0^1 p(c)dc=\frac{1}{N}\int_{c^-}^{c^+}\frac{1}{dc/d\xi}dc=\frac{1}{N}\int_{\xi^-}^{\xi^+}d\xi=\frac{\xi^+-\xi^-}{N}=1, \tag{9}$$

yielding $N = \xi^+ - \xi^- = \Delta_\xi$, which is true for any 1D laminar flame pdf. For constant c_p/λ, N is directly proportional to the filter width Δ_x in x space. The mean of any variable $z(c)$ evaluates as

$$\overline{z(c)}=\int_0^1 z(c)p(c)dc=\frac{1}{N}\int_{c^-}^{c^+}\frac{z(c)}{dc/d\xi}dc=\frac{1}{(\xi^+-\xi^-)}\int_{\xi^-}^{\xi^+}z(\xi)d\xi, \tag{10}$$

proving the validity of these results, since the last term represents the correct 1D spatial mean of z.

IV. EVALUATION OF FILTERED SOURCE TERM

Analytical evaluation of $\overline{\omega(c)}$ for a given $c(\xi)$ is always possible for a given analytical flame profile $c(\xi)$, using Eqs. (5) and (10),

$$\overline{\omega(c)} = \frac{1}{(\xi^+ - \xi^-)} \int_{\xi^-}^{\xi^+} \left(-\frac{\partial^2 c}{\partial \xi^2} + \frac{\partial c}{\partial \xi} \right) d\xi = \frac{1}{(\xi^+ - \xi^-)} \left[-\frac{\partial c(\xi)}{\partial \xi} + c(\xi) \right]_{\xi^-}^{\xi^+}. \quad (11)$$

An analytic inversion $\xi(c)$ of $c(\xi)$ allows us to convert the last term on the RHS into an expression depending on c instead of ξ. The lower and upper boundaries ξ^-, ξ^+ then translate into the lower and upper boundaries of the pdf, c^-, c^+.

The mean of the sum of laminar diffusion and reaction source terms used in many flame surface density models can be evaluated exactly for any 1D laminar flame pdf,

$$\overline{\frac{\partial^2 c}{\partial \xi^2} + \omega(c)} = \overline{\frac{\partial c}{\partial \xi}} = \frac{1}{(\xi^+ - \xi^-)} \int_{c^-}^{c^+} \frac{\overline{\partial c}}{dc/d\xi} dc = \frac{1}{(\xi^+ - \xi^-)} \int_{c^-}^{c^+} dc = \frac{(c^+ - c^-)}{(\xi^+ - \xi^-)}. \quad (12)$$

V. PRESUMED FLAME PROFILE

In a recent contribution,[25] an analytic invertible progress variable profile $c_m(\xi)$ was derived, which also provides an integrable source term $\omega_m(c)$ with a parameter m that can be adapted to different activation energy situations. This profile is generalized here slightly with the introduction of two additional constants C, a,

$$c_m(\xi) = \frac{C}{[1 + \exp(-a \cdot m \cdot \xi)]^{1/m}}. \quad (13)$$

The parameter a provides the possibility to rescale the ξ coordinate by a spatially constant factor, which will be useful in the representation of flame profiles of strained flames. The parameter C might represent the c value in the fully burnt state; however, later on, it is also used to represent the upper range of c values, which can be approximated by $c_m(\xi)$. Figure 1 shows the presumed flame profile and the corresponding source term $\omega(\xi)$ (scaled by a factor of 0.5 for clarity) for $m = 8$. Also shown is the source term $\omega(c)$ in c coordinates.

$c_m(\xi)$ can be inverted as

$$\xi_m(c) = -\frac{\log\left(\left(\frac{c}{C}\right)^{-m} - 1\right)}{a \cdot m}. \quad (14)$$

The spatial derivative of $c(\xi)$, expressed in c itself, is given by

$$dc/d\xi = a \cdot c(1 - (c/C)^m), \quad (15)$$

yielding a thermal flame thickness (which is the inverse of the maximum derivative) of

$$\delta_{th} = \frac{1}{(dc/d\xi)_{max}} = \frac{(m+1)^{\frac{m+1}{m}}}{a \cdot C \cdot m}. \quad (16)$$

For a constant stretch factor (i.e., $c_p/\lambda = \text{const.}$), the laminar flame pdf evaluates as

$$p(c) = \frac{1}{\Delta_\xi} \frac{1}{a \cdot c(1 - (c/C)^m)} H(c - c^-) H(c^+ - c), \quad (17)$$

with $\Delta_\xi = \left(\rho_u s_L c_p/\lambda\right) \cdot \Delta_x$. The chemical source term evaluates as

$$\omega_m(c) = a \cdot c(1 - (c/C)^m)(1 - a(1 - (c/C)^m(1 + m))), \quad (18)$$

with a mean value of

$$\overline{\omega_m(c)} = \int_0^1 \omega_m(c) p(c) dc = \frac{1}{N} \int_{c^-}^{c^+} \frac{\omega_m(c)}{dc/d\xi} dc. \quad (19)$$

For constant c_p/λ, we obtain

$$\overline{\omega_m(c)} = \frac{1}{\Delta_\xi} \int_{c^-}^{c^+} \left(1 - a(1 - (m+1)(c/C)^m\right) dc = \frac{1}{\Delta_\xi} \left[c(1 - a(1 - (c/C)^m))\right]_{c^-}^{c^+}. \quad (20)$$

For a filter interval in physical space with boundaries $[x^-, x^+]$, transforming into $[\xi^-, \xi^+]$, the limits of the integration evaluate as $c^- = c_m(\xi^-)$ and $c^+ = c_m(\xi^+)$. In the case $a = 1$, $C = 1$, Eq. (20) reduces to[25] the simple result

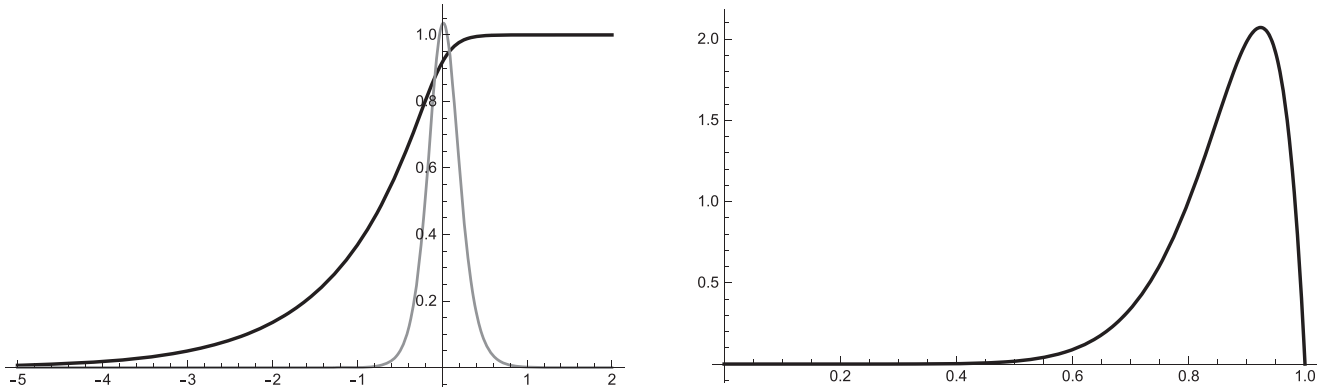

FIG. 1. Left: Presumed flame profile $c_m(\xi)$ (black) and source term $\frac{1}{2} \cdot \omega_m(\xi)$ (gray); right: source term $\omega_m(c)$.

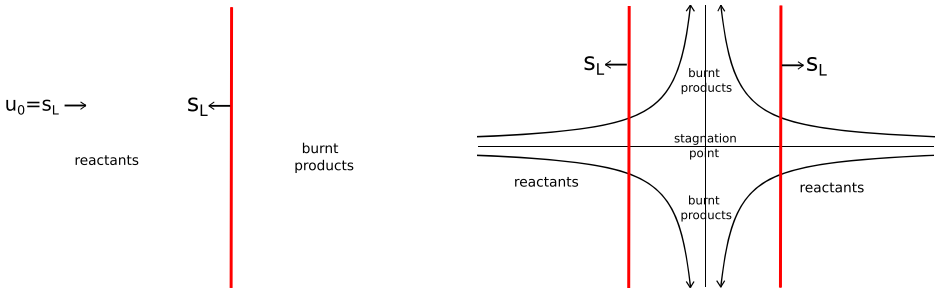

FIG. 2. Free flame (left) and counterflow flame (right) configurations.

$$\overline{\omega_m(c)} = \frac{1}{\Delta_\xi}\left((c^+)^{m+1} - (c^-)^{m+1}\right). \tag{21}$$

VI. GENERATION OF FLAME PROFILES

The methane–air laminar premixed flames are generated in this work using the software CANTERA[28] v. 2.4. The Gas Research Institute (GRI) mech 3.0[29] detailed chemical mechanism with the assumption of unity Lewis numbers was used in the calculations. The temperature of the unburnt mixture is set to $T_u = 300$ K, and combustion occurs at atmospheric conditions (p = 1 bar).

The freely propagating flat flames are calculated over a range of equivalence ratios ϕ varying from 0.4 to 2.2, on a 20 mm wide physical grid. Stretched premixed flames at equivalence ratios of $\phi = 1.0$ and $\phi = 0.6$ are calculated using a double premixed counter-flow flame configuration, where two identical, axially symmetric, premixed jets of fresh gases blow against each other. In these cases, the half-domain is 40 mm wide. The flame strain K varied from $K = 10$ to $K = 1000\,s^{-1}$ and was achieved by changing the inlet jet velocity U. The value of K is retrieved as the maximum of the local strain rates observed upstream, before the pre-heating zone.

Figure 2 shows the free flame and counter-flow double flame configurations. The red line represents the (flat) flame front, and the black lines in the counterflow configuration represent flow streamlines. The 1D flame profiles are calculated on the central axis of symmetry.

Figure 3 (left) reports the u profile across the steady free flame at $\phi = 1$, where the laminar flame speed s_L^0 is taken as the speed of the fresh gas retrieved at x = 0. In this example, the flame propagation speed $s_L^0 = 28.64$ cm/s. This value cannot be retrieved at the same location in the stretched flames since the velocity in x = 0 is the imposed inlet velocity, as shown on the right plot of Fig. 3. A local minimum is seen before the pre-heating zone (steep-increase in u), and its position moves toward the stagnation point (x = 40 mm) by increasing the strain K. The velocity drops to zero at the stagnation point.

In order to quantify the flame speed uniquely for both configurations, the flame consumption speed is used in this work. It is defined as the integral of the heat release rate across the flame brush,

$$s_c = \frac{1}{(T_b - T_u)\,\rho_u}\int \frac{\dot{Q}}{c_p}\,dx, \tag{22}$$

with ρ_u being the density of the unburnt mixture, T_b being the temperature of the burnt mixture, c_p being the mixture heat capacity at constant pressure, and $\dot{Q}$ being the total heat release rate.

The free flame s_c, generated with the assumption $Le_i = 1$, as a function of ϕ is shown in Fig. 4. Note that the s_c level is 10%–20% lower than s_L generated with differential transport, which is shown in many other publications/textbooks. The plot on the right shows how the laminar flame is affected by strain for $\phi = 1$ and 0.6. At higher strains, the consumption speed is slightly reduced, but it tends to the value calculated for the free flames by decreasing K, as expected.

Each stored flame profile contains additional scalars calculated at the grid points. The species progress variables (PVs) used in this work are defined as a linear combination of specific mole numbers. The specific mole number of the species k is defined as $\frac{Y_k}{W_k}$, with the mass fraction Y_k and the species molecular weight W_k.

A preliminary investigation showed that $PV_1 = CO_2 + CO$ representing carbon chemistry and $PV_2 = H_2O + H_2$ representing hydrogen chemistry appeared suitable progress variables due to a

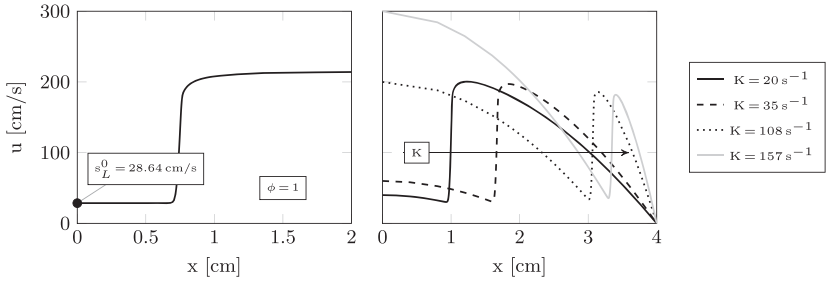

FIG. 3. Left: Laminar flame speed $s_L^0 = 28.64$ cm/s for a free flame at $\phi = 1$. Right: Stretched flames at different K for $\phi = 1$.

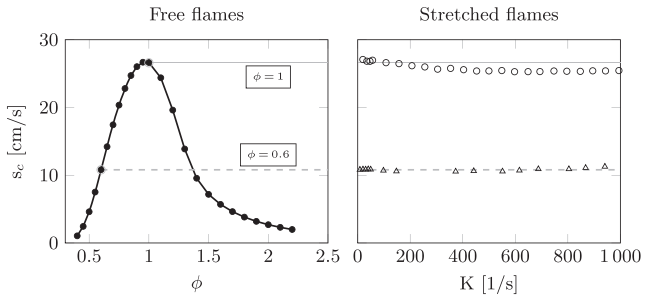

FIG. 4. Left: Free flame consumption speed s_c over the investigated ϕ range. Right: s_c for stretched premixed flames at $\phi = 0.6$ and 1, over an increasing range of K.

monotonous rise and positive source terms, which are calculated as $\omega_s = \sum_{i=1}^{n_r} \left(\frac{\dot{\omega}_i W}{\rho}\right)$, with n_r being the number species used to define the PV (therefore two in this work), $\dot{\omega}_i$ being the net production rate of the species i, and W being the mean molecular weight. The values of λ/c_p required in Eq. (4) and $\dot{Q}/c_p$ for Eq. (22) were stored in addition in the tables.

VII. ANALYSIS OF GRI mech 3.0 PROGRESS VARIABLES

In the first step, we investigated whether the analytic $c_m(\xi)$ flame profiles, which were developed in the context of single-step Arrhenius chemistry, could be suitable to also represent progress variable profiles derived from flame calculations with detailed chemistry and transport. In addition to the above-mentioned progress variables PV_1, PV_2, we investigated several other progress variables used in the literature (e.g., mass and mole fractions of CO_2, $CO_2 + CO$, H_2O, and $CO_2 + CO + H_2O + H_2$ and normalized temperature) for similarity to the single-step chemistry profiles.

Figure 5 shows the temperature and λ/c_p distributions of a $\phi = 1$ free flame in x space. The temperature distribution features a diffusive preheat zone and a steep reaction region that is followed by a long tail on the burnt side. The λ/c_p plot indicates that a strongly nonlinear stretch will occur within the flame front. We found that while most mass fraction and mole fraction combinations show a similar long tail on the burnt side like normalized temperature, which cannot directly be reproduced by $c_m(\xi)$, the above-mentioned combination of specific mole numbers (being the mass fraction divided by the corresponding molar weight) of $CO_2 + CO$ (representing carbon oxidation) and $H_2O + H_2$

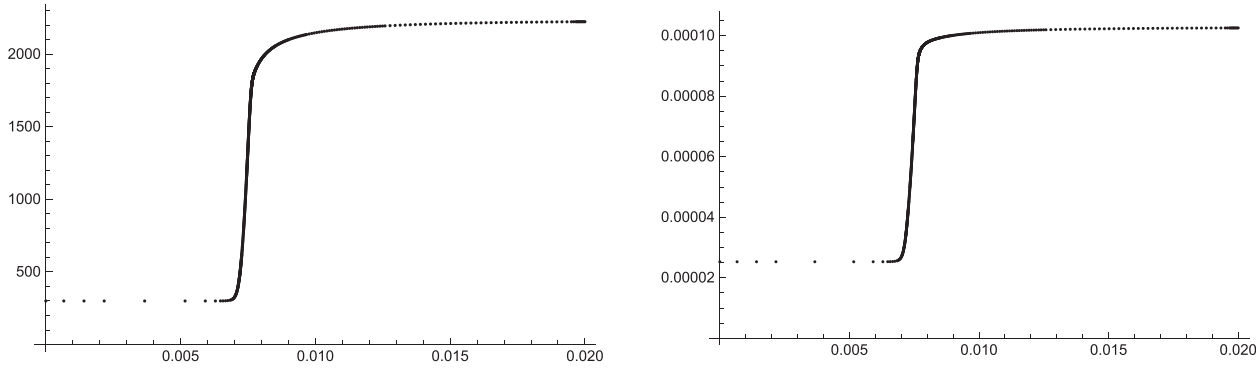

FIG. 5. Temperature (left) and λ/c_p (right) for a $\phi = 1.0$ free flame.

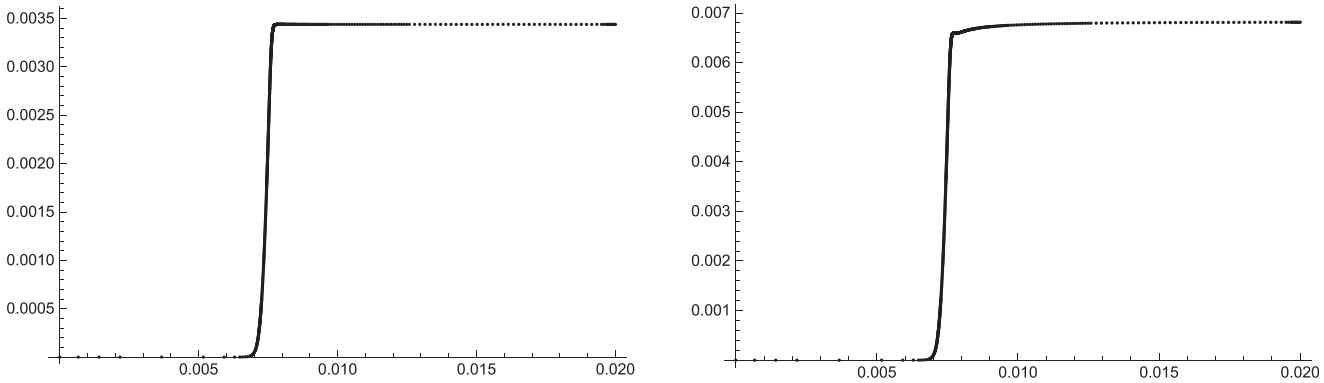

FIG. 6. Specific mole number of $CO_2 + CO$ (left) and $H_2O + H_2$ (right) for a $\phi = 1.0$ free flame.

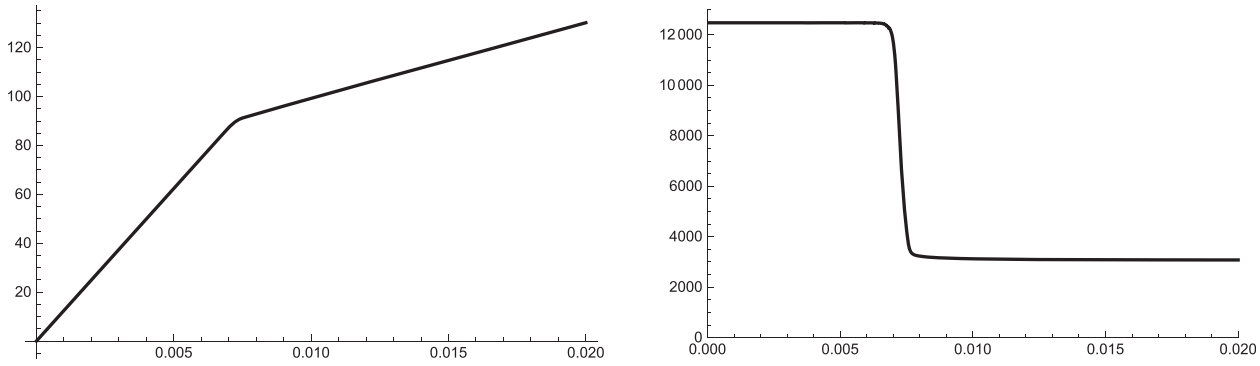

FIG. 7. Transformed coordinate $\xi(x)$ (left) and its derivative $d\xi/dx$ (right); $\phi = 1.0$.

(representing hydrogen oxidation) yielded profiles looking very similar to one-step chemistry, see Fig. 6. While $CO_2 + CO$ looks like a perfect match with one-step chemistry profiles, $H_2O + H_2$ additionally features a long tail on the burnt side, which in this case is, however, restricted to values very near $c = 1$.

In the presentation of results, we will focus on the analysis of $CO_2 + CO$ profiles. $H_2O + H_2$ yielded very similar results in the range $0 \leq c \leq C \approx 0.97$. We will also provide an analytical approximation of the c profile in the tail region applicable to $H_2O + H_2$ but also to other progress variables such as normalized temperature.

VIII. TRANSFORMATION OF FLAME PROFILES

As a next step, we evaluated the canonical transformation from the physical coordinate x to the canonical coordinate ξ where Eq. (5) is valid. Using the constant ρ_u, s_L and the variable $(c_p/\lambda)(x)$ from the detailed chemistry free flame calculations, Eq. (4) is integrated numerically yielding $\xi(x)$ shown in Fig. 7 for the case $\phi = 1.0$.

One can see that the derivative of $\xi(x)$ drops by a factor of 4 across the flame front mostly due to the increase in heat conductivity as temperature increases. The normalized $CO_2 + CO$ and $H_2O + H_2$ specific mole number profiles in the transformed coordinate ξ are shown in Fig. 8. Through the spatial coordinate transformation, the thickness of the preheat zone in ξ space becomes more pronounced compared to the profiles in x space.

Assuming that the c profiles in ξ coordinates fulfill Eq. (5), we can derive an equivalent effective source term $\omega(c)$ by numerically evaluating first and second derivatives of $c(\xi)$ and forming $\omega(\xi) = \partial c/\partial\xi - \partial^2 c/\partial\xi^2$. Parametric plots of $\omega(\xi)$ vs $c(\xi)$ yield the effective $\omega(c)$.

Such plots are shown in Fig. 9 for $CO_2 + CO$ and $H_2O + H_2$ progress variables. While $\omega(c)$ for $CO_2 + CO$ looks, indeed, very similar to the single-step one from Fig. 1, in case of $H_2O + H_2$, the one-step chemistry region appears to end at $c = C \approx 0.968$.

In the region between $c = C$ and $c = 1$, $\omega(c)$ for $H_2O + H_2$ can be roughly approximated by a linear function $\omega(c) \approx B(1 - c)$. Such a linear source term[24] also yields an analytical and invertible flame profile and pdf. The corresponding $c(\xi)$ solution of Eq. (5) is

$$c(\xi) = 1 + c_1 \cdot \exp\left[\frac{1}{2}(1 - \sqrt{1 + 4B})\xi\right] \tag{23}$$

discarding the term rising exponentially in ξ. c_1 is chosen for $c(\xi)$ to be continuous at $c = C$, and B can be selected to fit $\omega(c)$ in the region

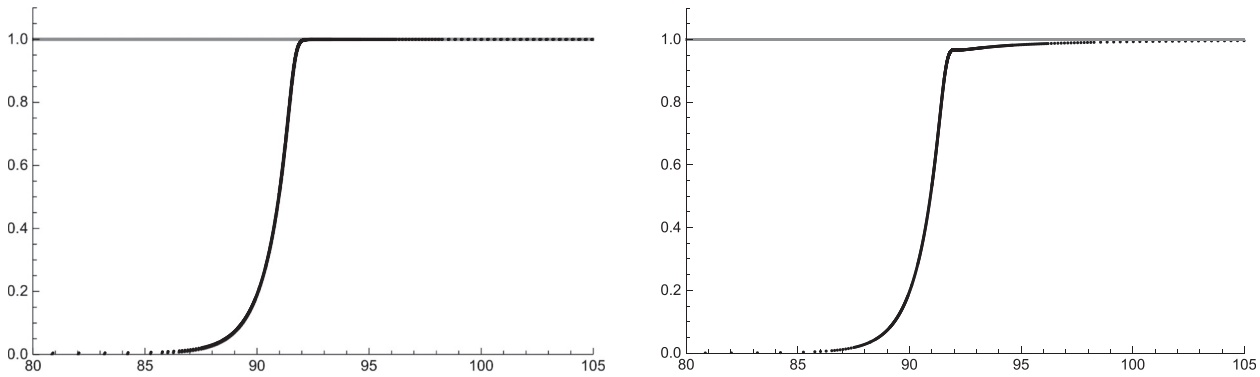

FIG. 8. Normalized specific mole number of $CO_2 + CO$ (left) and $H_2O + H_2$ (right) in the transformed coordinate ξ; free flame at $\phi = 1$.

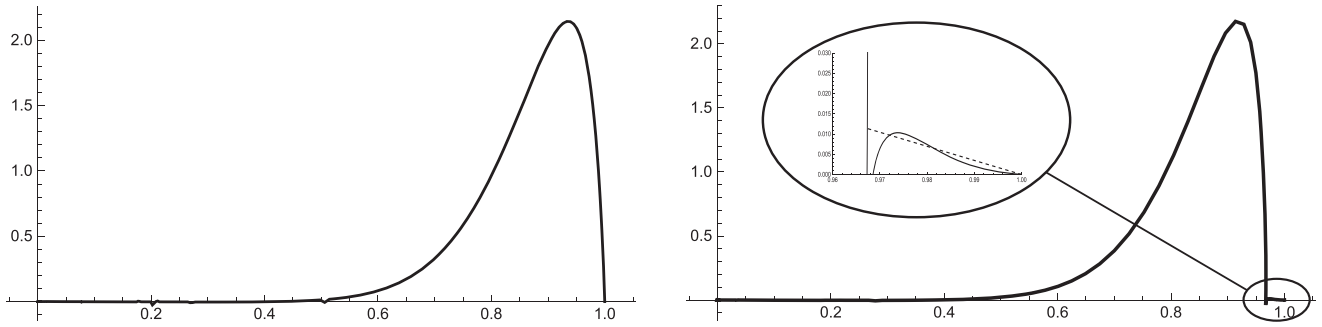

FIG. 9. Numerically generated $\omega(c)$ for $CO_2 + CO$ (left) and $H_2O + H_2$ (right); free flame at $\phi = 1$.

$C < c \leq 1$, see the inset in Fig. 9. For the pdf in this region, we need $dc/d\xi$ as a function of c. It evaluates as $dc/d\xi = \frac{1}{2}\left(\sqrt{4B+1} - 1\right)(1-c)$. When using a progress variable with a tail, the c profile and pdf are to be defined separately in the ranges $0 \leq c \leq C$ and $C \leq c \leq 1$. This makes calculations slightly more complicated, but the solutions are still analytical.

IX. DIRECT FIT OF $c(\xi)$ PROFILES

A direct least squares fit $c_m(\xi - \xi_0)$ to the GRI mech 3.0 distributions of $CO_2 + CO$ and $H_2O + H_2$ for $\phi = 1$ yields $a \approx 1$ in both cases and $m = 8.75$ and $m = 9.65$, respectively. The shift ξ_0 is irrelevant to the profile shape since the position of the GRI mech 3.0 profiles in x space is arbitrary.

Note that the preheat zone will only be reproduced accurately (with $a = 1$) with a consistent scaling factor $\rho_u s_L c_p/\lambda$. For example, the change in ρ_u due to the admixture of methane into air has to be considered properly. Figure 10 shows only the difference between the fitted $c_m(\xi)$ and GRI mech 3.0 profiles for $\phi = 1.0$ since an overlaid plot of fitted and GRI mech 3.0 profiles would not show any differences. The maximum difference is below 0.1% in both cases.

Using the normalized temperature as a progress variable, the fit yielded $m = 4.7$, $a = 0.95$, indicating that, for this progress variable, a much smaller effective activation temperature is required. The slightly smaller value of the stretch parameter a is caused here by the interaction between heat release and the varying effective molar weight within the preheat zone. The difference between the fitted $c_m(\xi)$ and GRI mech 3.0 profiles is similar as in the $CO_2 + CO$ and $H_2O + H_2$ cases in the preheat/reaction regions up to $c = C = 0.85$. The linear fit to $\omega(c)$ in the tail region $C \leq c \leq 1$ can also be applied here, but the difference between GRI mech 3.0 and fitted profiles rises up to 1% in this region.

Similar level reproduction of the GRI mech 3.0 profiles by $c_m(\xi)$ is achieved for lean flames down to $\phi = 0.4$ and for rich flames up to $\phi = 1.3$, see Fig. 11 for the case $\phi = 0.6$. Away from $\phi = 1$, the parameter m rises slightly, indicating that slightly different single-step Arrhenius effective activation temperatures are necessary for flames at different ϕ. The level of variation in the profile parameter m with ϕ is shown in Fig. 15, where m is determined from the flame speed distribution, retaining a close fit to the GRI 3.0 flame profiles.

For very rich flames (here $1.3 \leq \phi \leq 2.2$), the $CO_2 + CO$ specific mole number profiles develop a small long tail toward $c = 1$, while the tail tends to disappear from the normalized temperature profiles.

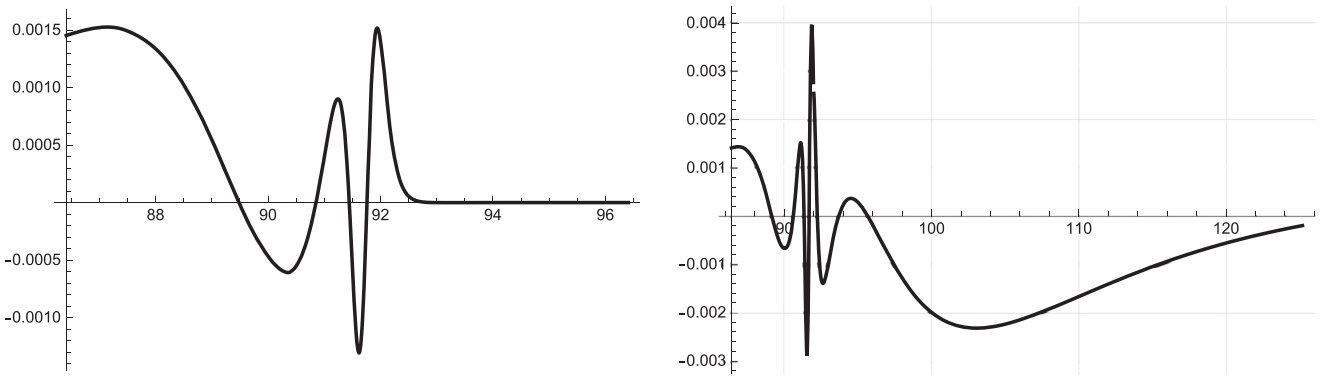

FIG. 10. Difference between fitted and GRI mech 3.0 profiles for $CO_2 + CO$ (left) and $H_2O + H_2$ (right); free flame at $\phi = 1$.

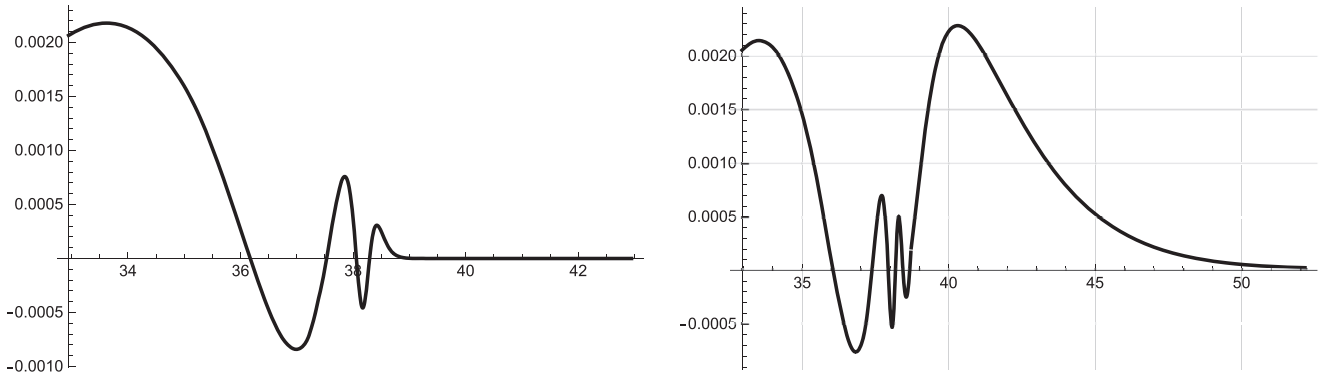

FIG. 11. Difference between fitted and GRI mech 3.0 profiles for $CO_2 + CO$ (left) and $H_2O + H_2$ (right); free flame at $\phi = 0.6$.

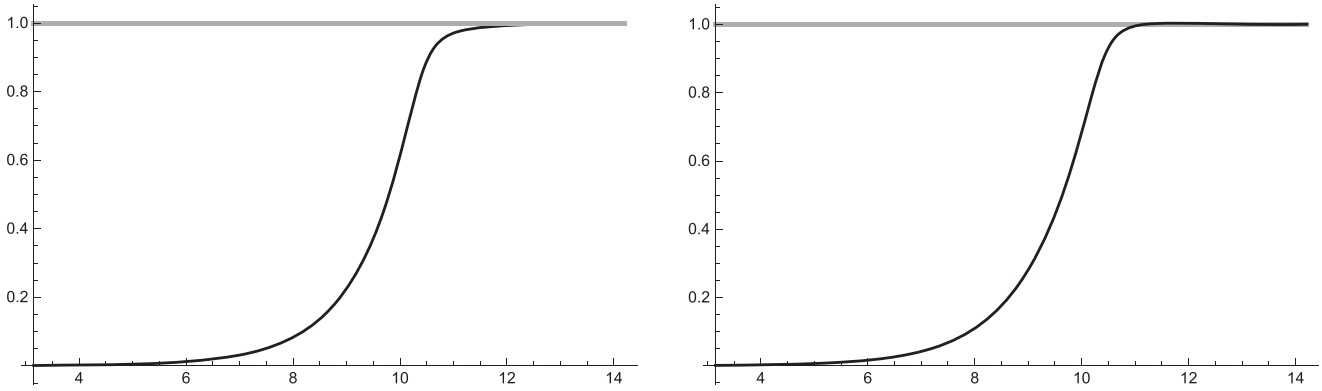

FIG. 12. Normalized specific mole number of $CO_2 + CO$ (left) and temperature (right) in the transformed coordinate ξ; free flame at $\phi = 2$.

Figure 12 shows transformed normalized $CO_2 + CO$ and temperature profiles for $\phi = 2$. Since, for Lewis numbers equal to one, the transport equations for species-derived progress variables and for normalized temperature are identical, a tabulation of flamelet quantities vs progress variables might use a $CO_2 + CO$ progress variable for $\phi < 1.3$ and switch to a table based on normalized temperature for richer flames.

X. ALTERNATIVE DETERMINATION OF PARAMETER *m*

In this section, we focus on an alternative derivation of the parameter m using T_u, $T_b(\phi)$ and $s_L(\phi)$ from the GRI mech 3.0 calculations only. We only present results for the $CO_2 + CO$ progress variable; the application of this method to the $H_2O + H_2$ and normalized temperature progress variables yields similar results.

In recent contributions,[25,26] we have derived analytical results for the laminar flame eigenvalue Λ in the case of single-step Arrhenius chemistry. We have also provided relations to evaluate the profile parameter m from the Arrhenius parameters α, β, β_1,

$$m = \frac{4}{5}(\alpha + \beta) - 1, \tag{24}$$

$$\Lambda = \frac{\beta^2}{2}\left(\frac{1-\alpha}{100} + 1\right) + 2\alpha\beta - \frac{22}{15}\beta. \tag{25}$$

Since results for $\beta_1 = 0$ and $\beta_1 = 1$ were very similar, we only present results for $\beta_1 = 0$.

Using $\alpha = (T_b - T_u)/T_b$ and $\beta = \alpha T_a/T_b$, we can first estimate an effective activation temperature of $T_a \approx 29\,200\ K$ for $\phi = 1$ using Eq. (24) and $m = 8.75$ from the fit to the $\phi = 1$ free flame profile. $T_u = 300$ K, and T_b is taken from the GRI mech 3.0 profiles, see Fig. 13. Note that T_b could also be calculated from equilibrium thermodynamics, since the fully burnt state of free flames should approach the thermodynamic equilibrium state.

For Arrhenius single-step chemistry, the laminar flame speed is[7]

$$s_L \propto \sqrt{T_b \exp\left(-\frac{\beta}{\alpha}\right)\Lambda} \tag{26}$$

up to constants independent of ϕ. For a constant activation temperature T_a, we can predict the ratio $s_L(\phi)/s_L(\phi = 1)$. The results are

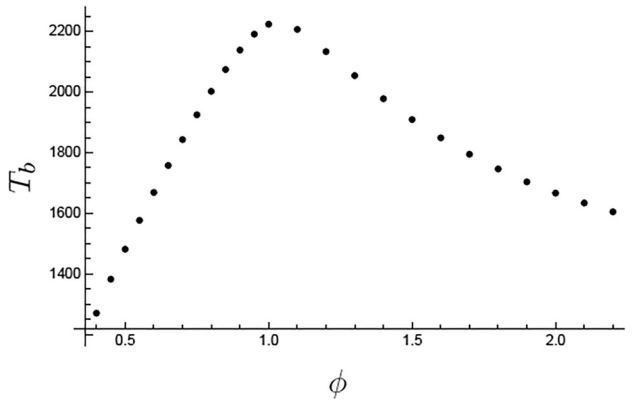

FIG. 13. T_b from GRI mech 3.0 free flame calculations.

shown in Fig. 14, left. We find that these predictions of $s_L(\phi)/s_L(\phi = 1)$ agree qualitatively with the GRI mech 3.0 results, but the precise value of s_L is very sensitive to the activation temperature T_a or, equivalently, m.

We, therefore, suggest to reverse the procedure, calculating an effective T_a or equivalently m for $\phi \neq 1$ from the GRI mech 3.0 $s_L(\phi)/s_L(1)$ and $T_b(\phi)$. The resulting m distribution is shown in Fig. 14(b) together with the m distribution evaluated for constant T_a. The slight change in m between the two distributions generates profiles that are hardly distinguishable. Obviously, using the adapted m's from Fig. 14(b) would bring the gray symbols in Fig. 14(a) exactly on top of the black ones.

The $c(\xi)$ profiles evaluated with m determined in this way also agree still very well with the detailed chemistry profiles, see Fig. 15. The difference is still below 0.4% and invisible in the plot on the left side of Fig. 15. For use in a CFD code, $s_L(\phi)$ and $m(\phi)$ calculated from $s_L(\phi)$, $T_b(\phi)$ can easily be represented by polynomials in ϕ.

XI. EFFECT OF STRAIN

To investigate whether the effect of strain on c profiles can also be represented by $c_m(\xi)$, we analyzed a series of strained GRI mech 3.0 laminar premixed flames strained in a counterflow unburnt–unburnt configuration at $\phi = 1$ and $\phi = 0.6$. Results for both ϕ's were qualitatively similar; therefore, we show only results for $\phi = 1$. Figure 16 displays T_b and s_L as a function of the strain rate K.

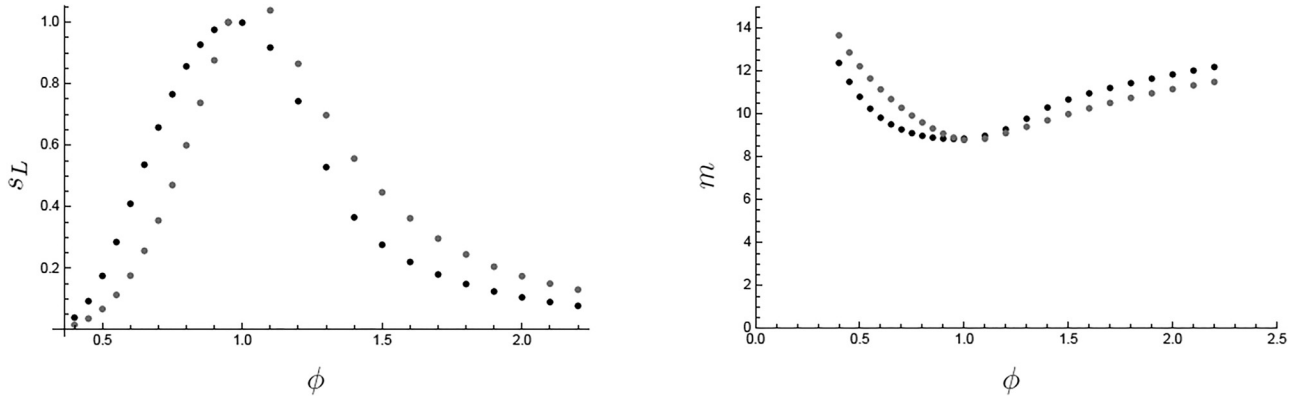

FIG. 14. Left $s_L/s_{L,\phi=1}$ from GRI mech 3.0 calculations (black) and calculated using constant T_a (gray); right: m for constant T_a (gray) and predicted using GRI mech 3.0 $s_L/s_{L,\phi=1}$ (black).

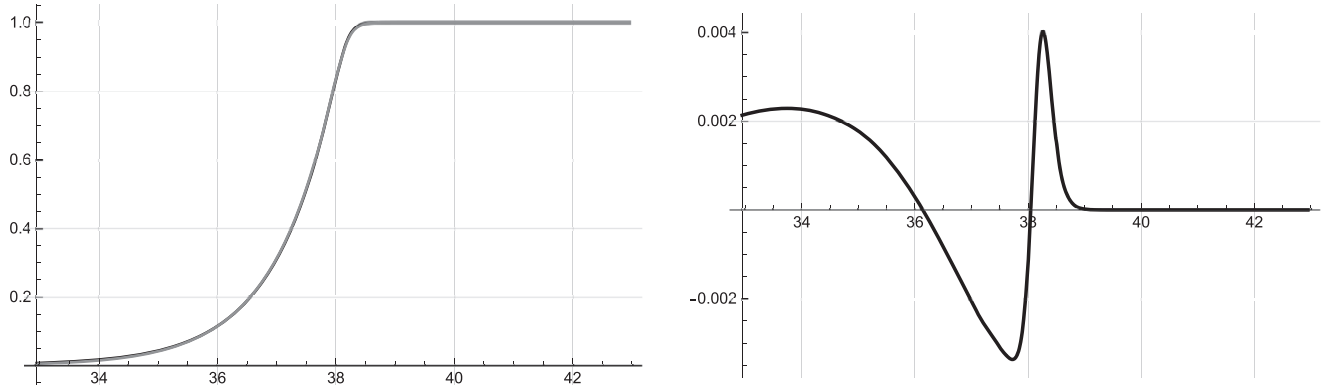

FIG. 15. Analytical (gray) and GRI mech 3.0 (black) $CO_2 + CO$ profiles (left) and difference (right); free flame at $\phi = 0.6$, m determined from s_L, T_b.

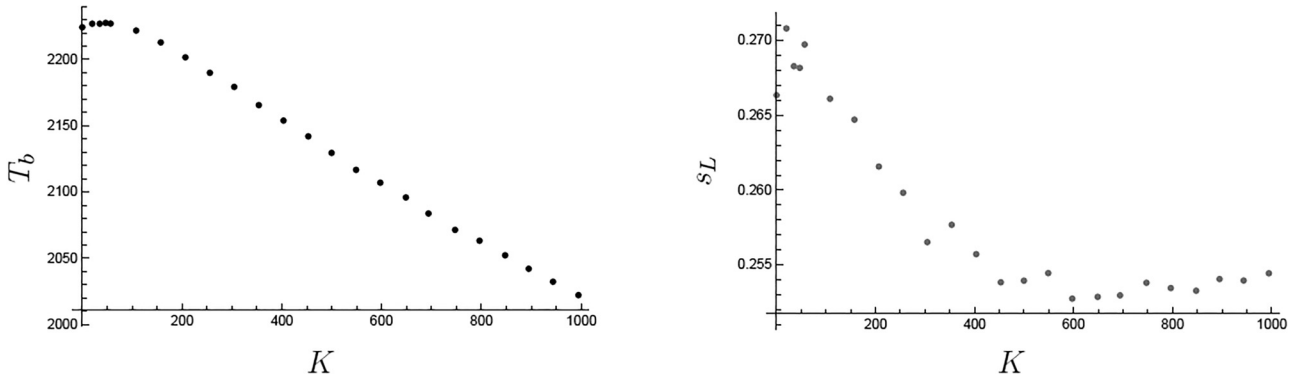

FIG. 16. GRI mech 3.0 burnt temperature (left) and laminar flame speed (right) of strained flames.

We find that, for these strained flames, the thermal flame thickness (evaluated as an inverse of the maximum derivative of the transformed detailed chemistry c profiles) is practically constant, independent of the strain level K. This is consistent with laminar flame theory,[30] which holds that the reaction zone will be almost unaffected by levels of strain away from the blow-off level. However, the preheat zone will be compressed compared to a free flame situation. Figure 17 (left) shows the GRI mech 3.0 profile with an analytic profile of the same thermal flame thickness and without additional compression (i.e., $a = 1$). It is evident that the preheat zone could not be reproduced by such $c_m(\xi)$.

The strained profiles, however, can be reproduced well by $c_m(\xi)$ when fitting m and a simultaneously. Figure 17(right) only shows the difference between the GRI mech 3.0 transformed profile and $c_m(\xi)$ for $\phi = 0.6$, $K = 688$. A stretch factor of $a = 1.50$ is required in this case to compress the preheat zone. The difference between GRI mech 3.0 and fitted profiles is again within 0.4%, as in the case of non-strained profiles. The stretch factor a required for preheat zone compression can be correlated as $a = (1 + 5.5 \cdot 10^{-5} \cdot Ka)$ with the Karlovitz number $Ka = K \cdot \delta_{th}^0 / s_L^0$, with δ_{th}^0 and s_L^0 evaluated from the unstrained flames. To retain the thermal thickness of the profiles for strained profiles with $a > 1$, the parameter m has to decrease with rising K. The fitted m values can be approximated as $m = m_{K=0} - \frac{3.9 \cdot K}{1000}$ for both $\phi = 1.0$ and $\phi = 0.6$.

XII. PREMIXED LAMINAR FLAME pdf WITH DETAILED CHEMISTRY AND NON-CONSTANT c_p/λ

The laminar flame pdf for constant c_p/λ is given by Eq. (8). For non-constant c_p/λ, the spatial region covered by a certain interval $d\xi$ is not constant, so spatial means in ξ space are not proportional to spatial means in x space.

A spatial mean of quantity z in x space for a filter of size Δ_x is defined as

$$\overline{z(x)} = \frac{1}{\Delta_x} \int_x^{x+\Delta_x} z(x) dx. \tag{27}$$

Since $d\xi = \rho_u s_L c_p / \lambda dx$, we can define a scaling function $R(x)$ through

$$\rho_u s_L (c_p/\lambda) = r_u / R(x), \tag{28}$$

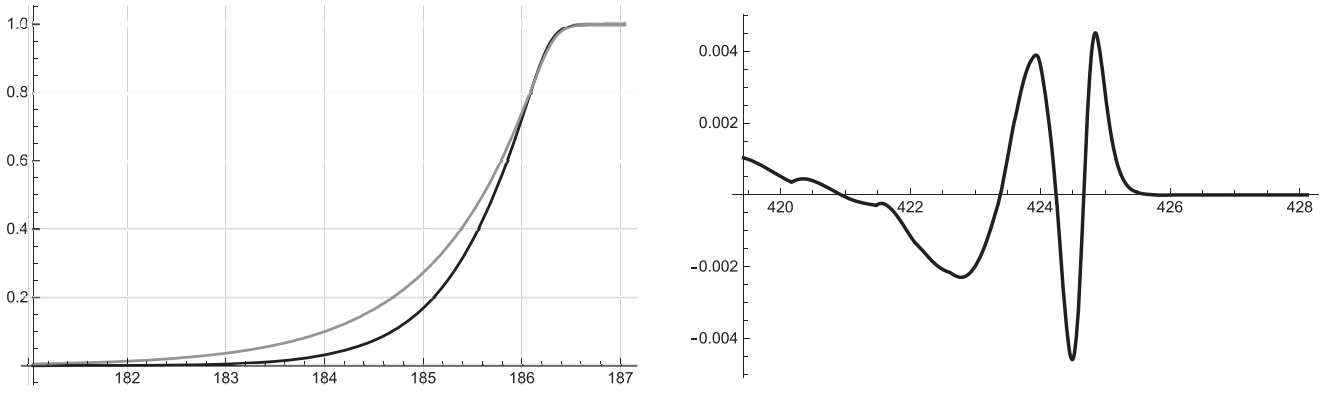

FIG. 17. Left: $c_m(\xi)$ with $a = 1$ (gray) and GRI mech 3.0 strained CO_2 + CO profile (black); right: difference between scaled GRI mech 3.0 and fitted profiles, $a = 1.5$; $\phi = 0.6$, $K = 688$.

where $r_u = \rho_u s_L (c_p/\lambda)_u$ is the stretch factor in the unburnt region. $R(x)$ is equal to one in this region and rises across the flame front.

Since $c(x)$ is monotonous in x, $R(x)$ can be transformed into $R(c)$, which is shown in Fig. 18 for the CO_2 + CO progress variable. If the last (almost vertical) portion of $R(c)$ is discarded (it will not contribute to the mean value of ω, which is zero at $c = 1$), $R(c)$ can very accurately be represented by a third order polynomial in c, the constant term being equal to one. The simple linear approximation $R(c) = 1 + c \cdot \frac{7}{10} \cdot \frac{r_u}{r_b}$, also shown in Fig. 18, yields only slightly less accurate results.

The integral in Eq. (27) can be evaluated as

$$\frac{1}{\Delta_x}\int_x^{x+\Delta_x} z(x)dx = \frac{r_u}{\Delta_\xi}\int_{\xi^-}^{\xi^+} \frac{z(\xi)}{d\xi/dx}d\xi = \frac{1}{\Delta_\xi}\int_{c^-}^{c^+} \frac{z(c)R(c)}{dc/d\xi}dc, \quad (29)$$

where $\Delta_\xi = \Delta_x \cdot r_u$ is to be evaluated using the stretch factor in the unburnt region. The integration limits ξ^-, ξ^+, c^-, c^+ are determined from x, Δ_x through $\xi^- = \xi(x)$, $\xi^+ = \xi(x + \Delta_x)$, $c^- = c(\xi^-)$, and $c^+ = c(\xi^+)$. Note that, with nonlinear stretching, $\xi^+ \neq \xi^- + \Delta_\xi$ with the above definition of Δ_ξ.

For a non-constant stretch factor, the laminar flame pdf becomes, therefore,

$$p(c) = \frac{1}{\Delta_\xi}\frac{R(c)}{dc/d\xi}H(c - c^-)H(c^+ - c). \quad (30)$$

Inserting $dc/d\xi$ as a function of c from Eq. (15), we see that, for the polynomial $R(c)$, all integrals required to evaluate $\overline{p(c)} = 1$, $\overline{c}$, and $\overline{\omega_m(c)}$ can be evaluated analytically using

$$I_0(c,m) = \int \frac{dc}{c(1-(c/C)^m)} = \log(c) - \frac{\log\left(1 - \left(\frac{c}{C}\right)^n\right)}{n}, \quad (31)$$

$$I_k(c,m) = \int \frac{c^k dc}{c(1-(c/C)^m)} = \frac{c^k\, {}_2F_1\left(1, \frac{k}{m}; \frac{k}{m}+1; \left(\frac{c}{C}\right)^m\right)}{k}, \quad (32)$$

where ${}_2F_1(a, b, c; x)$ is a hypergeometric function and $k \neq 0$ in Eq. (32). Note that $I_k(c,m) = \frac{I_1(c^k, m/k)}{k}$, so for numerical evaluation, only $I_1(c, m)$ is needed; a robust method[25] for numerical evaluation of this function was provided earlier.

Note also that, for the polynomial $R(c)$, $\frac{\omega_m(c)}{dc/d\xi}$ is a polynomial, see Eq. (20), even for detailed chemistry c profiles. In the case of the CO_2 + CO progress variable and ignoring the effect of strain for the evaluation of the mean source term (since strain will only affect the preheat region where ω is small), we have $a = C = 1$. Writing the polynomial expansion of $R(c)$ as

$$R(c) = 1 + \sum_{k=1}^{r} R_k c^k, \quad (33)$$

we obtain

$$1 = \int_0^1 p(c)dc = \frac{1}{N}\int_{c^-}^{c^+} \frac{R(c)}{c(1-c^m)} = \frac{1}{N}\left[\log(c) - \frac{\log(1-c^n)}{n} + \sum_{k=1}^{r} R_k I_k(c,m)\right]_{c^-}^{c^+}, \quad (34)$$

$$\overline{c} = \int_0^1 c \cdot p(c)dc = \frac{1}{N}\int_{c^-}^{c^+} \frac{cR(c)}{c(1-c^m)} = \frac{1}{N}\left[I_1(c,m) + \sum_{k=1}^{r} R_k I_{k+1}(c,m)\right]_{c^-}^{c^+}, \quad (35)$$

and

$$\overline{\omega} = \int_0^1 \omega_m(c) \cdot p(c)dc = \frac{1}{N}\int_{c^-}^{c^+} \frac{\omega_m(c)R(c)}{c(1-c^m)} = \frac{1}{N}\left[c^{m+1} + \sum_{k=1}^{r} R_k \frac{m+1}{m+k+1} c^{m+k+1}\right]_{c^-}^{c^+}. \quad (36)$$

The source term $\omega_x(c)$ in real space can be gained from $\omega(c)$ in ξ space as $\omega_x(c) = (\rho_u s_L)^2 \left(\frac{c_p}{\lambda}\right)_u \frac{1}{R(c)} \cdot \omega(c)$, see Eq. (6), where $R(c)$ takes into account the c variation of $\left(\frac{c_p}{\lambda}\right)$.

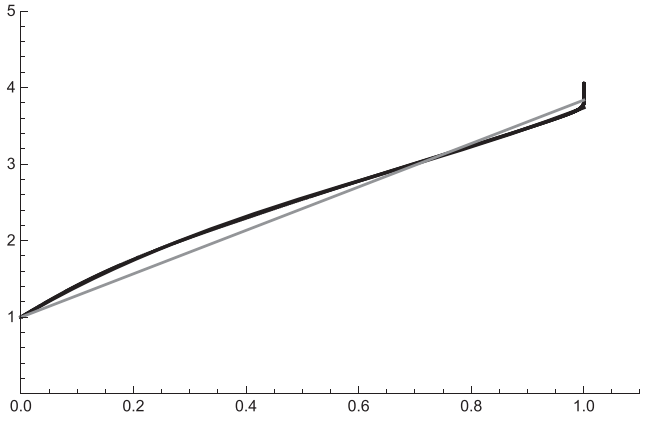

FIG. 18. Scaling factor as a function of c (black); also shown is linear approximation (gray).

XIII. ANALYTICAL APPROXIMATION OF $\xi(x)$

We have $c^- = c_m(\xi^-)$ and $c^+ = c_m(\xi^+)$, but for a non-constant stretch factor, the simple relation $\xi^+ = \xi^- + \Delta_\xi$ with $\Delta_\xi = r_u\Delta_x$ does not hold any more. It is, therefore, useful to have an explicit expression of $\xi(x)$. Using the approximation $c(\xi) = c_m(\xi)$ and the polynomial approximation to $R(c)$, one can integrate the differential equation

$$d\xi/dx = r_u/R(c_m(\xi)), \quad (37)$$

yielding the implicit equation

$$x - x_0 = \int_{\xi^-}^{\xi^+} \frac{R(c_m(\xi))d\xi}{r_u}. \quad (38)$$

Even with the linear approximation to $R(c)$, the integral on the RHS cannot be evaluated analytically.

As an alternative to numerical interpolation of $\xi(x)$, we provide an approximation to the derivative $d\xi/dx$ directly through a simple ansatz,

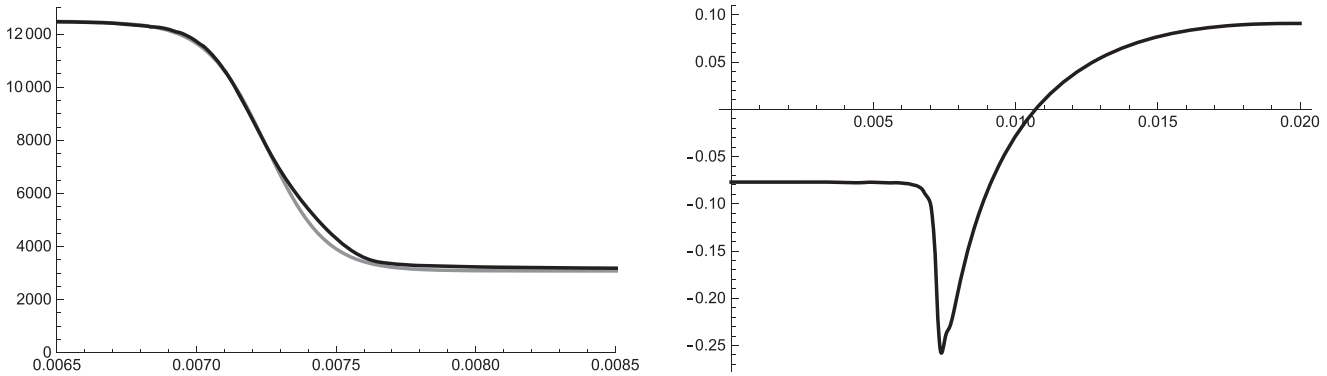

FIG. 19. Left: $d\xi/dx$ evaluated numerically (black), analytic approximation $d\xi_a/dx$ (gray); right: difference between real $\xi(x)$ and approximation $\xi_a(x)$.

$$r(x) = r_u + \frac{r_b - r_u}{1 + \exp(-3(r_u - r_b)(x - x_0)/5.} \tag{39}$$

This approximates real $d\xi/dx$ satisfactorily and yields the analytic approximation

$$\xi_a(x) = \xi_0 + \frac{5(r_b - r_u)\log\left(e^{\frac{3}{5}(r_b + r_u)(x - x_0)} + 1\right)}{3(r_b + r_u)} + r_u x, \tag{40}$$

where r_b is the value of $r(x)$ in the fully burnt region. Figure 19 shows a comparison of the $d\xi/dx$ profiles and the error in the reproduction of the $\xi(x)$ curve. Figure 7 shows the typical range of ξ values, so the approximation $\xi_a(x)$ is accurate to within 0.2%.

XIV. EVALUATION OF c^-, c^+, AND N

For application of the laminar flame pdf in a CFD code, the values of c^-, c^+ need to be evaluated for a given $\bar{c}$ (which is provided by a c transport equation) and a given filter Δ_x in x space. Due to the monotonicity of $c(x)$, $\bar{c}$ will be a monotonic function of x and Δ_x. Similar to Ref. 25, we propose the following preprocessing steps:

- Evaluate $\xi^- = \xi(x)$ and $\xi^+ = \xi(x + \Delta_x)$
- Evaluate $c^- = c_m(\xi^-)$ and $c^+ = c_m(\xi^+)$
- Evaluate N from Eq. (34) as a function of x, Δ_x
- Evaluate $\bar{c}$ from Eq. (35) using N and c^-, c^+
- Evaluate $\overline{\omega}$ from Eq. (36) using N and c^-, c^+

$p(c)$ as a function of x, Δ_x is now completely defined, so mean values of other quantities of interest $z(c)$ can be evaluated. Quantities N, c^-, c^+, and $\overline{\omega}$ might be re-tabulated as functions of $\bar{c}$ and filter size Δ_x for use in a CFD code.

XV. EFFECTS OF TURBULENT FLAME FOLDING ON $p(c)$

A turbulent flow field at low to moderate Karlovitz numbers will fold the laminar flame front without changing its inner structure noticeably. The simple model with sinusoidal flame folding[25] showed that the level of the pdf in the reactive c region will increase by a wrinkling factor Ξ while the pdf near c^-, c^+ is smeared out due to pushing in/out of parts of isosurfaces from the filter volume by flame folding. The mean reaction rate $\overline{\omega(c)}$ will mainly increase through a wrinkling factor Ξ. A similar behavior was observed from analysis of DNS data.[17,19,20] At higher Karlovitz numbers into the corrugated/thin reaction zone regime, a stronger mixing of the preheat zone will occur through small turbulent eddies.

The exact relationships[25] evaluated in x space provide

$$p(c) = \frac{1}{\Omega_x}\int_{\Omega_x} \delta(c(\vec{x}) - c)d\vec{x}. \tag{41}$$

The c isosurface area density within the volume Ω_x is given by

$$\sigma(c) = \frac{1}{\Omega_x}\int_{\Omega_x} \delta(c(\vec{x}) - c)|\nabla c(\vec{x})|d\vec{x}, \tag{42}$$

and a correction factor $I(c)$ can be defined as

$$I(c) = \frac{\frac{1}{\Omega_x}\int_{\Omega_x} \delta(c(\vec{x}) - c)|dc/dx|_{1D,c}d\vec{x}}{\sigma(c)}, \tag{43}$$

yielding

$$p(c) = \frac{\sigma(c) \cdot I(c)}{|dc/dx|_{1D,c}}, \tag{44}$$

where Ω_x is the filter volume in real space. $I(c)$ represents the effect of the mean difference between the local c gradient and the one of the 1D flat flame.

With a nonlinear transformation, Eq. (44) becomes

$$p(c) = \frac{\sigma(c) \cdot I(c) \cdot R(c)}{r_u \cdot |dc/d\xi|_{1D,c}}. \tag{45}$$

Analysis of DNS data of turbulent plane premixed flames at $u'/s_L = 5$, 15[26] has shown that, despite considerable flame folding, $I(c)$ and $\sigma(c)$ are rather constant in c for large, RANS-type filter volumes. $I(c)$ was near one, and the level of $\sigma(c)$ rised proportionally to the flame wrinkling intensity. The role of the cutoffs c^-, c^+ of the 1D case is taken into account through the c dependence of $\sigma(c)$ in a three-dimensional (3D) setting. $\sigma(c)$ then drops continuously to zero near c^-, c^+.

The pdf of the reaction layer in a thin folded flame can be approximated by the 1D laminar flame pdf through use of a reduced filter width $\Delta' = \Delta/\Xi$, where Ξ is a wrinkling factor,

$$p_\Xi(c, \Delta) = p_{1D,\Xi=1}(c, \Delta' = \Delta/\Xi), \tag{46}$$

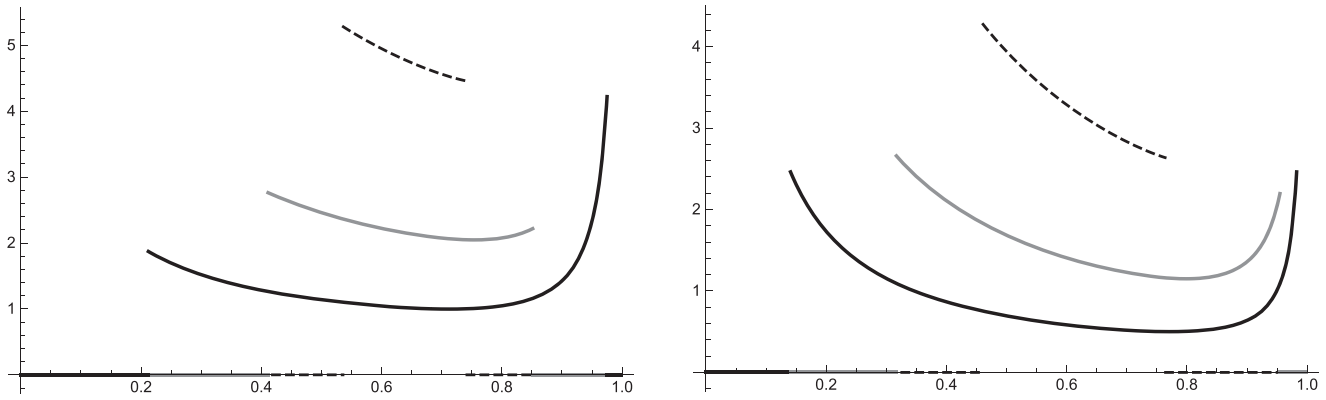

FIG. 20. $p(c)$ for $\overline{c} = 0.6$, $\Delta_x = 240\ \mu$, and $\phi = 1$ (black), $\phi = 0.6$ (gray), and $\phi = 0.5$ (dashed). Left: Full c_p/λ; right: $c_p/\lambda = (c_p/\lambda)_u$.

where also c^-, c^+ are evaluated with a filter scaled by $1/\Xi$. This will automatically raise the level of the pdf in the range of c^-, c^+, and the evaluation of c^-, c^+ using $\Delta' = \Delta/\Xi$ will ensure the correct normalization of $p(c)$.

XVI. pdf OF PARTIALLY PREMIXED FLAMES

In the case of thin flame fronts propagating through a fuel–air mixture with a locally (slowly) varying mixture fraction Z, a common model for the joint pdf $p(Z, c)$ is based on application of Bayes's theorem,[31,32]

$$p(Z, c) = p_Z(Z) \cdot p(c|Z), \tag{47}$$

where $p_Z(Z)$ is the marginal pdf of the mixture fraction and $p(c|Z)$ is the pdf of c conditional on the mixture fraction, which is modeled as a 1D laminar premixed flame pdf at $\phi(Z) = \frac{Z}{1-Z} \cdot \frac{Z_{st}}{1-Z_{st}}$ corresponding to the respective mixture fraction. This assumes that the inner structure of the propagating flame fronts is little affected by the spatial variation of Z.

$p_Z(Z)$ is commonly modeled as a β function,

$$p_Z(Z) = p_\beta(Z) = \frac{Z^{a-1}(1-Z)^{b-1}\Gamma(a+b)}{\Gamma(a)\Gamma(b)}, \tag{48}$$

with parameters a, b evaluated from a transport equation of mixture fraction Z and its variance. In LES, the latter is sometimes also evaluated from an algebraic model.

The conditional pdf $p(c|Z)$ modeled as a laminar premixed flame pdf is then given by

$$p(c|Z) = \frac{1}{N_Z}\frac{R_Z(c)}{dc_{m_Z}/d\xi} H(c - c_Z^-) H(c_Z^+ - c), \tag{49}$$

with $m(Z)$, $R_Z(c)$ and c^-, c^+ evaluated at $\phi(Z)$. In the 3D case, the conditional pdf would read

$$p(c|Z) = \frac{\sigma_Z(c) \cdot I_Z(c) \cdot R_Z(c)}{|dc_{m_Z}/d\xi|_{1D,c}}. \tag{50}$$

Again, for the low to moderate Karlovitz numbers one can expect $I_Z(c) \approx 1$ in the reactive c region. $\sigma(c)$ will be dominated by wrinkling of large turbulent eddies; its cutoff regions will depend on the ratio of filter volume Ω_x to laminar flame thickness $\delta_{th}(Z)$. Since the latter grows as ϕ moves away from $\phi = 1$, a smaller subgrid isosurface density can be expected in lean regions compared to near-stoichiometric ones. Since the maximum of c_p/λ varies only by 30% over the investigated ϕ range (mainly in the lean region), the stretch factor is dominated by the ϕ variation of s_L. Inspection of Fig. 13 shows that a flame at $\phi = 0.5$ is six times wider than a stoichiometric flame.

A certain filter interval Δ_x in x space then translates into a smaller Δ_ξ in ξ space, and c^-, c^+ are nearer to $\overline{c}$ for lean/rich flames than for stoichiometric ones. Figure 20 shows 1D unstrained flame pdf's at $\phi = 1$, 0.6, 0.5 in a cell of width $\Delta_x = 240\ \mu$ and for $\overline{c} = 0.6$ using the full nonlinear $R(c)$ (left) and using $R(c) = 1$ (right), i.e., performing the coordinate transformation using the unburnt c_p/λ only. The pdf's for the leaner flames cover a much smaller range $[c^-, c^+]$ in transformed ξ coordinates than the stoichiometric one. Note, however, that application of a wrinkling factor Ξ will raise the pdf level and narrow its range, so a partial correction of the difference can occur. Figure 21 shows a comparison of the shape of the non-normalized pdf $R(c)/(dc/d\xi)$, scaled with the full polynomial $R(c)$, using a constant value $R(c) = 1 + \frac{2}{3}(R(1) - 1)$ and using the linear approximation

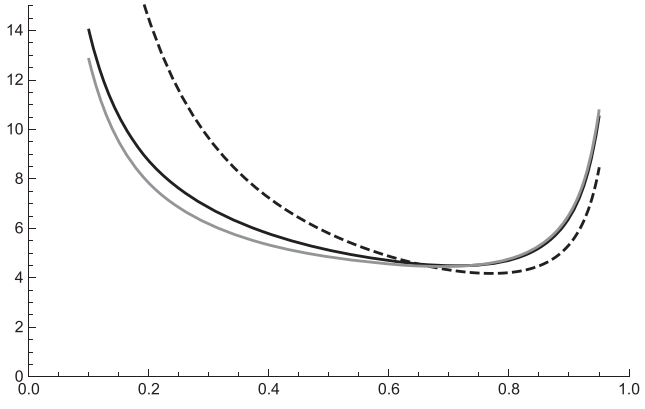

FIG. 21. $R(c)/(dc/d\xi)$; black: full nonlinear $R(c)$, dashed: $R(c) = 1 + \frac{2(R(1)-1)}{3}$ = const., and gray: $R(c) = 1 + \frac{7r_u}{10r_b}c$.

$R(c) = 1 + \frac{7r_u}{10r_b}c$. The shape of the pdf cannot be recovered using a constant R, while a quite good approximation is possible with the linear approximation to $R(c)$.

XVII. ANALYTICAL PARTIALLY PREMIXED FLAME pdf FOR CONSTANT c_p/λ

A fully explicit analytic pdf $p(Z, c)$ can be formulated in the case that c_p/λ depends only on the mixture fraction Z but does not change across the flame. We present this here to demonstrate the main ingredients of the pdf and because this form can be applied directly in the evaluation of DNS data that use this assumption.

Assuming a beta pdf for a marginal pdf of the mixture fraction and a laminar flame pdf for $p(c|Z)$ filtered with $\Delta' = \Delta/\Xi$, we obtain

$$p(Z,c) = \frac{Z^{a-1}(1-Z)^{b-1}\Gamma(a+b)}{\Gamma(a)\Gamma(b)} \cdot \frac{\Xi}{\rho_u s_L(Z)(c_p/\lambda)_u \cdot \Delta_x} \cdot \frac{1}{c(1-c^{m(Z)})} H(c-c^-)H(c^+-c), \tag{51}$$

where parameters a, b of the beta pdf for Z are evaluated from the Z mean and variance, $s_L(Z)$ and $m(Z)$ are preprocessed functions of Z as indicated above, and c^-, c^+ are calculated similarly to the purely premixed case from $\overline{(c|Z)}$ and the effective filter width $\Delta'_\xi = \rho_u s_L(Z)(c_p/\lambda)_u \cdot \Delta_x/\Xi$. The c^-, c^+ correlation provided in Ref. 25 might be used as an approximation. The wrinkling factor Ξ might be evaluated from models developed in the framework of ATFs or FSD models or from a transport equation of the c variance, using the Filtered Laminar Flame (FLF) pdf method to evaluate $\Delta' = \Delta/\Xi$. Also here, it should be considered that the subgrid flame wrinkling factor is expected to increase with increasing Δ/δ_{th}, so Ξ should be higher in regions $\phi \approx 1$ than that in very lean or very rich regions with larger δ_{th}.

For small, LES-typical filter widths, the smearing of the 3D pdf near c^-, c^+ is noticeable, see pdf's shown in Refs. 19, 20, and 25. For larger, RANS-like filter volumes, the effect is minor since c^-, c^+ are very near $c = 0$, 1 and the smear-out of the pdf in this region has only a small effect on most mean values.

XVIII. APPLICABILITY OF PARTIALLY PREMIXED MODEL pdf

It can be expected that this analytic partially premixed flame pdf, multiplied by an appropriate factor accounting for the effect of subgrid flame wrinkling, should be a good approximation to the pdf in the reactive c region, if inverse gradients of the mixture fraction are much larger than the premixed flame thickness. This should be the case for many turbulent partially premixed flames of interest in technical applications such as gas turbines or internal combustion engines combustors.

Many wrinkling factor models are available in the literature in the framework of flame surface density models, but the applicability of such models to the presented model pdf needs further investigation. An alternative would be the evaluation of the scaling factor following the procedure by Moureau,[19] using a subgrid c variance evaluated from its transport equation or from an algebraic model. In addition, this procedure needs further validation through *a priori* and *a posteriori* investigations of both RANS and LES type filter volumes.

Note that the structure of flamelet pdf's as investigated here implies that propagating flame fronts have already formed. These model pdf's do not apply to situations where autoignition or local flame extinction effects are of importance (although a delta function like pdf can be created using a very small effective filter width). The effect of flame strain will compress the preheat zone and change the pdf there, but its effect on the filtered reaction rate might be small for low to moderate strain, since, in this regime, the strain hardly changes the fuel consumption rate[30] and the structure of the inner reaction zone. Additional investigations are also necessary to substantiate these assumptions and to clarify their range of applicability.

XIX. CONCLUSIONS AND OUTLOOK

In this contribution, we have shown that the progress variable distribution of the CO_2 + CO and H_2O + H_2 specific mole number combinations in free premixed laminar flame profiles generated with the GRI mech 3.0 detailed chemistry mechanism using real transport coefficients can be represented very accurately by a slight generalization of recently proposed analytical flame profiles after a canonical stretch of coordinates.

The model parameter m of the analytical profiles in transformed coordinates can be calculated very accurately using the laminar flame speed and the burnt temperature only, using results from single-step Arrhenius chemistry theory. The results indicate that slightly different effective activation temperatures for the Arrhenius model are required to reproduce flame profiles at different fuel/air ratios ϕ.

Profiles of strained flames can also be reproduced accurately after application of an additional linear coordinate transformation. The stretch parameter a is found to be a linear function of the Karlovitz number. As expected from combustion theory, the activation temperature and the thermal flame thickness are approximately independent of the strain level in the investigated range of K.

The analyses permit the derivation of an analytical presumed laminar flame pdf for detailed chemistry premixed methane flames (Le = 1) at different fuel/air ratios. The effect of a nonlinear c_p/λ on the pdf is derived. The mean progress variable $\bar{c}$, the c variance and $\overline{\omega}$ can be evaluated analytically also this case. We also provide an analytic approximation of $\xi(x)$.

We discuss modifications of the pdf due to turbulence shortly and propose an analytical pdf $p(Z, c)$ based on the application of Bayes's theorem for the case of propagation of thin flames into non-homogeneous mixtures with a slowly varying mixture fraction. The marginal pdf of the mixture fraction is approximated by a beta function, while the pdf of c conditional on Z is represented by pdf's of premixed laminar flame profiles at ϕ corresponding to the local Z. The slow variation of Z translates into the assumption of negligible effects from cross-diffusion of the mixture fraction between different c profiles, i.e., $|\nabla c| \gg |\nabla Z|$ in the reaction region. This is a good assumption in many applications featuring such flames.

The next steps will be the validation of the proposed detailed chemistry pdf's using DNS data of fully premixed flames generated with the same detailed chemistry mechanism and transport. The partially premixed analytic pdf will be first validated with DNS databases of flames propagating into the non-homogeneous mixture using single-step Arrhenius chemistry. The final step will be the validation of the pdf of partially premixed flames with detailed chemistry using suitable DNS databases.

Further investigations are planned to derive/validate models of the wrinkling factor Ξ and the subgrid flame surface density $\sigma(c)$ and, if necessary, the correction factor $I(c)$. Ξ models developed in the framework of flame surface density and ATF-type models will be the starting point.

We will also investigate the suitability of models of the subgrid variance, which showed some promise to determine the wrinkling factor using the FLF pdf method. *A posteriori* simulations will be performed on DNS and experimental configurations. Extensions of the approach to cases with more than one progress variable will be sought.

AUTHORS' CONTRIBUTIONS

P.B. generated the GRI mech 3.0 premixed flame profiles and data. M.P. performed all other analyses.

ACKNOWLEDGMENTS

The authors would link to thank M. Klein and N. Chakraborty for fruitful discussions. They also gratefully acknowledge the funding of part of this work by the Deutsche Forschungsgemeinschaft under Project Nos. PF443/9-1 and KL1456/5-1.

The authors confirm that ethical standards have been obeyed.

The authors declare that they have no conflict of interest.

DATA AVAILABILITY

The data that support the findings of this study are available from the corresponding author upon reasonable request.

REFERENCES

[1]J. F. Driscoll, "Turbulent premixed combustion: Flamelet structure and its effect on turbulent burning velocities," Prog. Energy Combust. Sci. **34**, 91–134 (2008).

[2]S. Luca, A. Attili, E. L. Schiavo, F. Creta, and F. Bisetti, "On the statistics of flame stretch in turbulent premixed jet flames in the thin reaction zone regime at varying Reynolds number," Proc. Combust. Inst. **37**, 2451–2459 (2019).

[3]T. Nilsson, H. Carlsson, R. Yu, and X.-S. Bai, "Structures of turbulent premixed flames in the high Karlovitz number regime - DNS analysis," Fuel **216**, 627–638 (2018).

[4]F. Proch, P. Domingo, L. Vervisch, and A. M. Kempf, "Flame resolved simulation of a turbulent premixed bluff-body burner experiment. Part I: Analysis of the reaction zone dynamics with tabulated chemistry," Combust. Flame **180**, 321–339 (2017).

[5]O. Colin, F. Ducros, D. Veynante, and T. Poinsot, "A thickened flame model for large eddy simulations of turbulent premixed combustion," Phys. Fluids **12**, 1843–1863 (2000).

[6]H. Pitsch and L. D. de Lageneste, "Large-eddy simulation of premixed turbulent combustion using a level-set approach," Proc. Combust. Inst. **29**, 2001–2008 (2002).

[7]T. Poinsot and D. Veynante, *Theoretical and Numerical Combustion*, 2nd ed. (Edwards, 2005).

[8]T. Ma, O. T. Stein, N. Chakraborty, and A. M. Kempf, "A posteriori testing of algebraic flame surface density models for LES," Combust. Theory Modell. **17**, 431–482 (2013).

[9]B. Fiorina, R. Vicquelin, P. Auzillon, N. Darabiha, O. Gicquel, and D. Veynante, "A filtered tabulated chemistry model for LES of premixed combustion," Combust. Flame **157**, 465–475 (2010).

[10]P. Domingo and L. Vervisch, "Large eddy simulation of premixed turbulent combustion using approximate deconvolution and explicit flame filtering," Proc. Combust. Inst. **35**, 1349–1357 (2015).

[11]K. Bray, M. Champion, P. Libby, and N. Swaminathan, "Finite rate chemistry and presumed PDF models for premixed turbulent combustion," Combust. Flame **146**, 665–673 (2006).

[12]E. Knudsen, S. H. Kim, and H. Pitsch, "An analysis of premixed flamelet models for large eddy simulation of turbulent combustion," Phys. Fluids **22**, 115109 (2010).

[13]P. Domingo, L. Vervisch, S. Payet, and R. Hauguel, "DNS of a premixed turbulent V flame and LES of a ducted flame using a FSD-PDF subgrid scale closure with FPI-tabulated chemistry," Combust. Flame **143**, 566–586 (2005).

[14]M. M. Salehi and W. K. Bushe, "Presumed PDF modeling for RANS simulation of turbulent premixed flames," Combust. Theory Modell. **14**, 381–403 (2010).

[15]M. M. Salehi, W. K. Bushe, N. Shahbazian, and C. P. Groth, "Modified laminar flamelet presumed probability density function for LES of premixed turbulent combustion," Proc. Combust. Inst. **34**, 1203–1211 (2013).

[16]B. Jin, R. Grout, and W. K. Bushe, "Conditional source-term estimation as a method for chemical closure in premixed turbulent reacting flow," Flow, Turbul. Combust. **81**, 563–582 (2008).

[17]H. P. Tsui and W. K. Bushe, "Linear-eddy model formulated probability density function and scalar dissipation rate models for premixed combustion," Flow, Turbul. Combust. **93**, 487–503 (2014).

[18]A. W. Skiba, C. D. Carter, S. D. Hammack, and J. F. Driscoll, "Experimental assessment of the progress variable space structure of premixed flames subjected to extreme turbulence," Proc. Combust. Inst. (published online, 2020).

[19]V. Moureau, P. Domingo, and L. Vervisch, "From large-eddy simulation to direct numerical simulation of a lean premixed swirl flame: Filtered laminar flame-PDF modeling," Combust. Flame **158**, 1340–1357 (2011).

[20]S. Lapointe and G. Blanquart, "A priori filtered chemical source term modeling for LES of high Karlovitz number premixed flames," Combust. Flame **176**, 500–510 (2017).

[21]A. Lipatnikov and V. Sabelnikov, "Evaluation of mean species mass fractions in premixed turbulent flames: A DNS study," Proc. Combust. Inst. (published online, 2020).

[22]A. N. Lipatnikov, V. A. Sabelnikov, F. E. Hernández-Pérez, W. Song, and H. G. Im, "A priori DNS study of applicability of flamelet concept to predicting mean concentrations of species in turbulent premixed flames at various Karlovitz numbers," Combust. Flame **222**, 370–382 (2020).

[23]A. N. Lipatnikov, V. A. Sabelnikov, F. E. Hernández-Pérez, W. Song, and H. G. Im, "Prediction of mean radical concentrations in lean hydrogen-air turbulent flames at different Karlovitz numbers adopting a newly extended flamelet-based presumed PDF," Combust. Flame **226**, 248–259 (2021).

[24]J. H. Ferziger and T. Echekki, "A simplified reaction rate model and its application to the analysis of premixed flames," Combust. Sci. Technol. **89**, 293–315 (1993).

[25]M. Pfitzner, "A new analytic PDF for simulations of premixed turbulent combustion," Flow, Turbul. Combust. (published online, 2020).

[26]M. Pfitzner and M. Klein, "A near-exact analytic solution of progress variable and PDF for single-step Arrhenius chemistry," Combust. Flame **226**, 380–395 (2021).

[27]M. Hansinger, M. Pfitzner, and M. Klein, "Statistical analysis and verification of a new premixed combustion model with DNS data," Combust. Sci. Technol. **192**, 2093–2114 (2020).

[28]D. Goodwin, R. Speth, H. Moffat, and B. Weber, "Cantera: An object-oriented software toolkit for chemical kinetics, thermodynamics, and transport processes," https://www.cantera.org, 2018.

[29]G. Smith, D. Golden, M. Frenklach, N. Moriarty, B. Eiteneer, M. Goldenberg, C. Bowman, R. Hanson, S. Song, W. Gardiner, V. V. Lissianski, and Z. Qin, "GRI-Mech—An optimized detailed chemical reaction mechanism for methane combustion," Report No. GRI-95/0058, Gas Research Institute, Berkeley, USA, 1995.

[30]A. Lipatnikov, *Fundamentals of Premixed Turbulent Combustion* (CRC Press, 2012).

[31]D. Dovizio and C. B. Devaud, "Doubly conditional source-term estimation (DCSE) for the modelling of turbulent stratified V-shaped flame," Combust. Flame **172**, 79–93 (2016).

[32]A. N. Lipatnikov and V. A. Sabelnikov, "An extended flamelet-based presumed probability density function for predicting mean concentrations of various species in premixed turbulent flames," Int. J. Hydrogen Energy **45**, 31162–31178 (2020).